

# Self-organisation processes in the carbon arc for nanosynthesis

J. Ng and Y. Raitses

*Princeton Plasma Physics Laboratory, Princeton, New Jersey 08543, USA*

(Received 19 November 2014; accepted 15 January 2015; published online 13 February 2015)

The atmospheric pressure carbon arc in inert gases such as helium is an important method for the production of nanomaterials. It has recently been shown that the formation of the carbon deposit on the cathode from gaseous carbon plays a crucial role in the operation of the arc, reaching the high temperatures necessary for thermionic emission to take place even with low melting point cathodes. Based on observed ablation and deposition rates, we explore the implications of deposit formation on the energy balance at the cathode surface and show how the operation of the arc is self-organised process. Our results suggest that the arc can operate in two different ablation-deposition regimes, one of which has an important contribution from latent heat to the cathode energy balance. This regime is characterised by the enhanced ablation rate, which may be favourable for high yield synthesis of nanomaterials. The second regime has a small and approximately constant ablation rate with a negligible contribution from latent heat. © 2015 Author(s). All article content, except where otherwise noted, is licensed under a Creative Commons Attribution 3.0 Unported License. [<http://dx.doi.org/10.1063/1.4906784>]

## I. INTRODUCTION

Carbon arcs, first discovered in the early 19th century,<sup>1</sup> have had numerous applications. They have been used as radiation standards,<sup>2</sup> in image furnaces<sup>3</sup> and in carbon arc welding among other things. A recent development has been their use as an efficient method for the production of high purity carbon nanotubes,<sup>4–6</sup> in which the graphite anode ablates and nanotubes and other fullerenes are formed in a deposit on the cathode surface.<sup>5,7</sup> As nanotubes have unique electrical and mechanical properties,<sup>8–10</sup> they could potentially be used for hydrogen storage, nanoelectronics, chemical sensors, and many other applications.<sup>8,9,11</sup>

It has been proposed<sup>12–14</sup> and was recently shown<sup>15</sup> that the carbonaceous deposit (which contains nanotubes) formed during the carbon arc discharge plays a crucial role in its operation. The deposit (1) changes the arc from graphite-cathode to graphite-deposit, (2) reaches the high temperatures necessary for thermionic emission to provide the electron current, and (3) reduces heat flux to the cathode.

Figure 1 illustrates the self-organisation process, in which the steady-state operation of the carbon arc is treated as a self organised process. Electrons emitted from the carbonaceous deposit heat the graphite anode, which ablates. The carbon ions and atoms travel to the cathode and condense to form the deposit, which is at the high temperature necessary for thermionic emission to support the electron current in the arc.

The ablation and deposition during the arc should be accounted for in models as the deposit formation changes the cathode material, which affects the arc-cathode interaction. In our experiments, under similar operating conditions, we show that the arc can operate in two ablation-deposition regimes in which the importance of deposition in the energy balance at the cathode changes drastically. In particular, in the regime with enhanced ablation and deposition which is relevant to nanosynthesis, the latent heat is an important

term in the energy balance at the cathode. This regime is important for synthesis of nanomaterials such as nanotubes, which are produced from atoms, ions, and molecules of the ablated anode material (e.g., graphite). The synthesis yield is thus determined by the ablation rate.

This paper is organised as follows: In Sec. II, we describe the experiments which demonstrate the existence of the two ablation-deposition regimes and provide data for the energy balance calculations. We also provide a brief analysis of the deposits formed. Section III is a discussion of a model of energy balance at the surface of the cathode, and we show the importance of considering deposition in the regime with enhanced ablation. Finally, the results are summarised and discussed in the final section.

Although the focus of this paper is on the carbon arc, the results may be applicable to other anodic arcs (in which the anode evaporates) where a solid deposit is formed on the cathode such as the arc for the synthesis of boron nitride and hybrid B-C-N nanotubes.<sup>16</sup>

## II. EXPERIMENTS AND RESULTS

### A. Setup

Using the setup described in previous works,<sup>15,17</sup> experiments were performed with a copper cathode of diameter 50 mm and graphite anodes with diameter between 6 and 12 mm in order to determine electrode temperatures and ablation rates. Helium at 500 Torr was used as a buffer gas. The duration of each experiment was approximately 1 min,

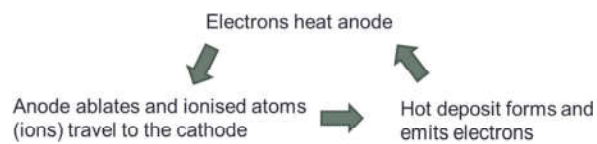


FIG. 1. Schematic of self-organisation in the carbon arc.



with discharge current 65 A. Arcing was initiated by bringing the anode into contact with the cathode, after which the control system would increase the electrode separation until the specified arc voltage was reached. The graphite anode would ablate and form a carbonaceous deposit on the cathode.

The electrode separation was controlled by maintaining the voltage in the external circuit between 20 and 25 V using a feedback system. With the 6 mm anode, the voltage was approximately 25 V, while with the 12 mm anode, it was approximately 21 V. The discharge voltage was approximately 20 V for the 6 mm anode arc and 18 V for the 12 mm arc after subtracting the resistance of the circuit elements and carbon deposit. These values were due to the feedback system causing the arcs to stabilize at different voltages. Temperature measurements were performed during arc operation, while the ablation and deposition rates were determined after each run.

## B. Ablation and deposition rates

Ablation and deposition rates were measured by weighing the electrodes before and after arc operation. The deposits grown were roughly circular with diameter 7–9 mm. With the 6 mm diameter anode, deposits would grow until the arc extinguished, while with the 12 mm diameter anode deposits did not exceed 1 mm in thickness.

Deposition rates were between 0.6 and 0.7 of the ablation rate, independent of anode diameter. This is likely due to the arc gap of 1–2 mm being much smaller than the electrode diameters, which would reduce the loss of material from the inter-electrode gap.

The ablation rates are shown in Figure 2. Above diameters of 9 mm, the ablation rate was small (<1 mg/s) and approximately constant, while at smaller diameters, the ablation rate rose abruptly. In addition, there were visible craters on the anodes with diameters >8 mm, indicating that the arc diameter was smaller than the anode diameter. These observations are consistent with Ref. 17, in which enhanced ablation was observed at smaller anode diameters. The lower ablation rates observed with larger anodes are caused by

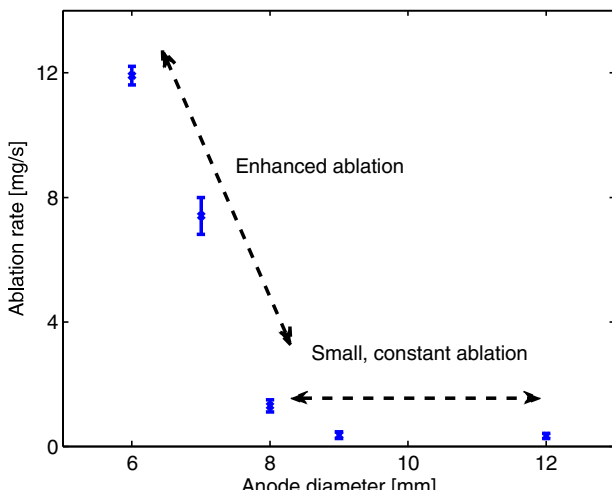


FIG. 2. Anode ablation rates.

larger radial heat loss, and the enhanced ablation with smaller anodes has been attributed to the increased current density and the possibility of the existence of a positive anode sheath.<sup>17</sup> Increasing the total current in the arc causes larger ablation and deposition rates to be observed.<sup>17,18</sup>

## C. Deposit structure

The deposits formed on the cathode had diameter 7–9 mm and were roughly circular, with length depending on the anode size and ablation rate. For the experiments used in this paper, the deposit with the 6 mm anode was 10 mm long while with the 12 mm anode it was 0.5 mm long. An *ex-situ* analysis of the carbon deposits with 6 and 12 mm diameter anodes was performed in Ref. 15, and we briefly summarise the key results based on scanning electron microscope (SEM) imaging, Raman spectroscopy, and X-ray diffraction (XRD).

In both cases, deposits were porous and less dense than graphite ( $1.34 \pm 0.06 \text{ g/cm}^3$  for the 6 mm anode and  $0.8 \pm 0.2 \text{ g/cm}^3$  for the 12 mm anode). From the SEM images, the deposit morphology varied spatially and consisted of flat, tubular, spherical, and chain-like particles.<sup>15</sup> These results are consistent with other studies of the cathode deposit.<sup>12,19</sup> Raman spectra displayed the two typical peaks at  $1340 \text{ cm}^{-1}$  and  $1590 \text{ cm}^{-1}$ , which correspond to the D and G bands. The ratio of the intensity of the D-band to G-band was generally higher on the side facing the cathode than the side facing the plasma, indicating spatial variation of the deposit structure with more defects on the cathode-facing side.<sup>15</sup> X-ray diffraction patterns revealed a shifting of the (002) and (004) peaks to lower angles, indicating larger interlayer spacings consistent with the presence of nanotubes.<sup>20</sup>

## D. Temperature measurements

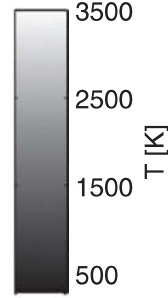
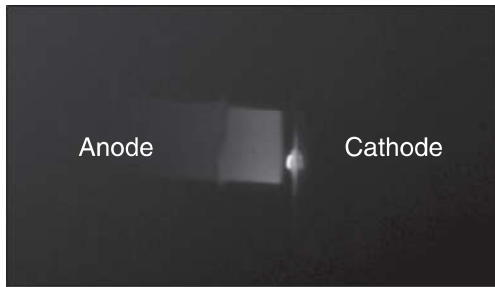
For the temperature measurements, a FLIR Tau 640 1.7 infrared camera was used together with a 3.2% transmittance neutral density filter. Absolute calibration of the camera was performed using arcs between graphite electrodes in conjunction with C-type thermocouples embedded in the electrodes. Figure 3 shows the cathode temperatures as measured by an infrared camera. The surface temperatures reach up to 3500 K in the case with the copper cathode, which allows thermionic emission to support the current in the arc.

For the measurements within the electrodes, thermocouples were placed 3 and 8 mm behind the exposed surface of a 10 mm diameter graphite cathode, as shown in Fig. 4. The results are shown in Figure 5. In the figure, the squares are the thermocouple measurements, while the temperature distribution is obtained by solving the one-dimensional heat equation<sup>21</sup>

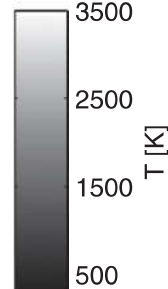
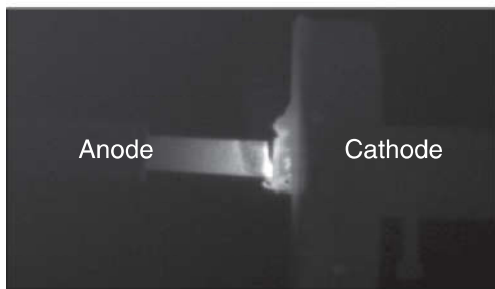
$$\pi r^2 j^2 \rho = 2\pi r h \Delta T + 2\pi r \sigma \epsilon T^4 - \pi r^2 \frac{\partial}{\partial x} \left( \kappa \frac{\partial T}{\partial x} \right) \quad (1)$$

within the cathode, where from left to right, the ohmic heating is balanced against convection, radiative cooling, and thermal conduction. Here,  $r = 5 \text{ mm}$  is the radius of the cathode used in the experiment,  $j$  is the current density,  $\rho$  is the

(a) 12 mm diameter graphite anode and copper cathode



(b) 6 mm diameter graphite anode and copper cathode



resistivity of graphite,  $\epsilon$  is the emissivity assumed to be 0.8,<sup>22</sup> and  $\kappa$  is the temperature dependent thermal conductivity of graphite.<sup>23</sup> The heat transfer coefficient  $h$  is given by  $K_{He}Nu/r$  where  $Nu$  is the Nusselt number, and  $\Delta T = T - T_0$  where  $T_0 = 300$  K. For the cases, we study here, the average Nusselt number is approximately 1.1 and ranges from 1 to 1.2 locally. This quantity is small as the density of the gas decreases, while kinematic viscosity increases with temperature, causing the Rayleigh number to be small. The results of our calculations are consistent with our previous infrared measurements and the literature.<sup>15,22</sup>

In order to extrapolate to the surface of the deposit interacting with the plasma for the case of the 6 mm diameter anode, Equation (1) can be integrated to the deposit surface. Figure 6 shows the results using different material parameters for the deposit. In Fig. 6(a), the deposit is assumed to be graphite, giving a heat flux at the surface of 439 W, and a surface temperature of approximately 2900 K.

This calculation is sensitive to thermal conductivity and emissivity. Reducing emissivity reduces the calculated temperature at the cathode surface and heat flux, while reducing thermal conductivity of the deposit increases the calculated surface temperature and heat flux. Figure 6 shows the effect of varying these parameters. For example, in Fig. 6(b), the emissivity is kept at 0.8, while thermal conductivity is taken as that of graphite at approximately 2100 K, while in Fig.

FIG. 3. Infrared measurements of the cathode deposit on copper cathode with (a) 12 mm diameter anode and (b) 6 mm diameter anode.

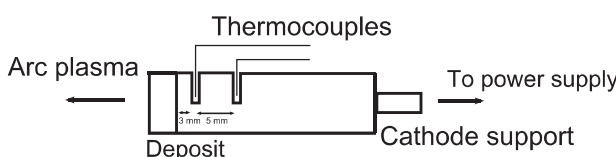


FIG. 4. Sketch of thermocouple positioning within the cathode.

6(c), the emissivity is reduced to 0.5 while keeping the conductivity the same.

To determine appropriate values of  $\kappa$  and  $\epsilon$  for the deposit, a parameter scan in  $\kappa$  and  $\epsilon$  was performed in order to match the observed surface temperatures by solving Eq. (1), assuming their values are temperature independent. In order to have a surface temperature of 3300 K, we find that  $\kappa$  of the deposit must be between 13 and 20 W/m/K, with  $\epsilon$  depending on the exact value of  $\kappa$ . The range of values here is consistent with graphite at high temperatures.<sup>23</sup>

Due to the difficulty in obtaining emissivity data relevant to the deposit produced in this experiment, we compare

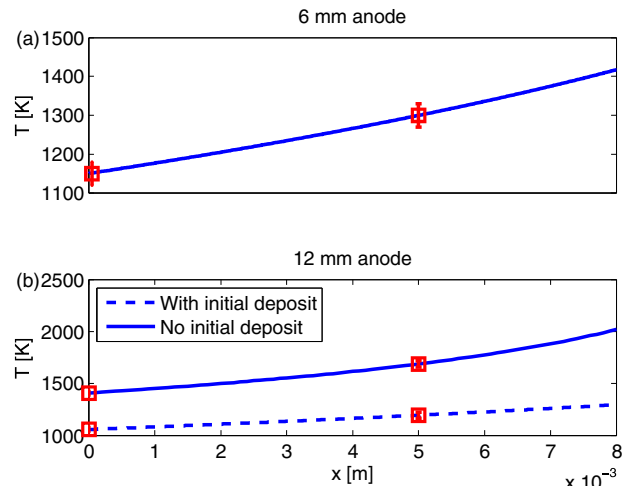


FIG. 5. Temperature measurements and calculated distribution within the cathode. (a) Using the 6 mm anode, with a 10 mm deposit formed on the cathode. (b) Using a 12 mm anode. The solid line is from an experiment using a cathode with an existing 10 mm deposit, while the dashed line is for the case using a cathode with no initial deposit. The thermal conductivity of graphite is taken from Ref. 23 and the emissivity is assumed to be 0.8.<sup>22</sup>

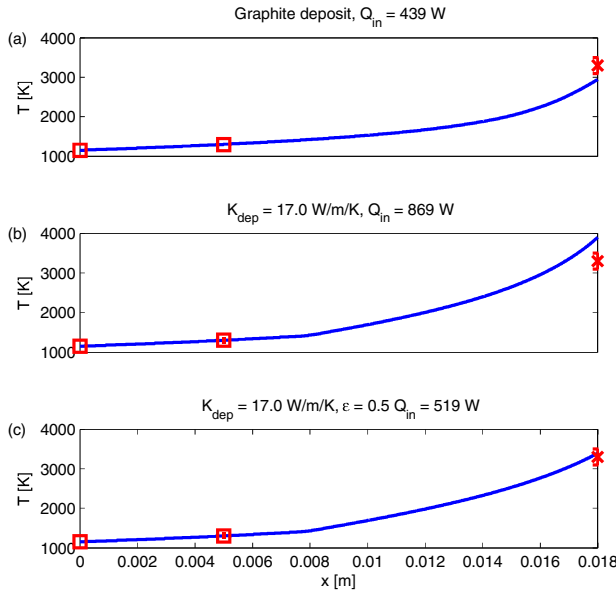


FIG. 6. Variation of calculated temperature, heat flux into the deposit  $Q_{in}$  with material parameters of deposit. (a) Graphite deposit, (b)  $\kappa = 17 \text{ W/m/K}$ ,  $\epsilon = 0.8$  (c)  $\kappa = 17 \text{ W/m/K}$ ,  $\epsilon = 0.5$ . The squares are thermocouple measurements while the x's are surface temperatures from the infrared measurements.

our deposit to carbon dust produced during discharges in fusion reactors, which was found to have a similar structure to deposits formed during arc discharges.<sup>24</sup> The source of this dust is the graphite used in the divertor plates of the reactors. A study of the removal of such plasma-deposited carbon determined its emissivity to be 0.5.<sup>25</sup> However, as the emissivity strongly depends on the structure and surface properties, and the deposit structure varies spatially, we use a range of values in our analysis. The heat flux into the deposit from the surface is between 280 and 640 W. A more accurate analysis will require knowledge of the material properties of the deposit and their temperature dependence.

For the situation with the 12 mm anode and the small deposit, the heat flux at the surface is between 260 and 300 W after performing the parameter scan. The required deposit thermal conductivity to match the measured surface temperatures is approximately 1 W/m/K. The low value of thermal conductivity has been observed in amorphous hydrocarbon films,<sup>26</sup> and differences in thermal conductivity from the deposit formed with the 6 mm anode can be attributed to the different structure and density observed.<sup>15</sup>

### III. CONTRIBUTION OF DEPOSIT TO CATHODE ENERGY BALANCE

The one-dimensional energy balance at the cathode is given by<sup>21,27</sup>

$$\begin{aligned} & \frac{j_i}{e} (E_i + eV_c - \phi) + \kappa_{He} \frac{dT_{He}}{dx} + F_{ac} \epsilon^2 \sigma T_a^4 + JH \\ & \quad (1) \qquad (2) \qquad (3) \qquad (4) \\ & = \kappa_c \frac{dT_c}{dx} + \frac{j_{ee}}{e} (2T_e + \phi) + \epsilon \sigma T_c^4. \\ & \quad (5) \qquad (6) \qquad (7) \end{aligned} \quad (2)$$

Here,  $j_i$  is the ion current density at the cathode,  $E_i$  the ionisation energy,  $V_c$  the sheath voltage drop,  $\phi$  the work function of the cathode material,  $T_i$  and  $\kappa_i$  the temperatures and conductivities of the subscripted materials,  $J$  the flux of deposited material (from both neutrals and ions) and  $H$  the latent heat of vapourisation of carbon.

$F_{ac}$  is the view factor which determines what fraction of the anode radiation reaches the cathode

$$F_{ac} = \frac{1}{2} \left( X - \sqrt{X^2 - 4 \left( \frac{R_c^2}{R_a^2} \right)} \right), \quad (3)$$

here  $R = r/d$ ,  $X = 1 + (1 + R_c^2)/R_a^2$ , and  $d$  and  $r$  are the electrode separation and radius respectively.

Heat flux to the surface is described by the first line of the equation. From left to right, the terms describe (1) ion heating with electron work function subtracted as they are required to neutralise the ions, (2) heating due to conduction from the carbon-helium plasma, (3) anode radiation, and (4) deposition. We have neglected the contribution from the back current of electrons  $\frac{1}{4} n_e v_{Te} \exp(-V_c/T_e)(2T_e + \phi)$  as it is exponentially suppressed with  $V_c/T_e > 5$  in our experiment with  $V_c > 3 \text{ V}$  and  $T_e \approx 0.6 \text{ eV}$ .<sup>17</sup>

The terms in the last line are cooling due to (5) heat conduction into the cathode, (6) electron emission, and (7) radiation from the cathode.

The presence of the deposit causes the energy balance at the cathode to differ from typical arcs operating in the spot mode due to the additional heating from deposition.<sup>28</sup> In our analysis, we consider two cases: a 6 mm anode and 10 mm graphite cathode with a deposit of thickness 10 mm, and a 12 mm anode with a 10 mm graphite cathode and a deposit of thickness 0.5 mm, as they correspond to most closely to the experiments in which the temperature within the cathode was measured.

We assume  $T_a = 3915 \text{ K}$ , the sublimation point of graphite,  $T_c = 3300 \text{ K}$  from the experiment,  $\phi = 4.6 \text{ eV}$  for the deposit, which we assume is similar to the value for graphite. Based on data from the infrared camera and graphite cathodes, a smaller region of the cathode deposit is heated when a 12 mm anode is used (Fig. 3 and Ref. 15). With the 12 mm anode, the heated area had diameter 6 mm, while with the 6 mm anode, we use a diameter of 8 mm. In the case of the 6 mm anode, we only consider the central deposit and ignore the “collar” that forms around it. Heat conduction in the cathode deposit is determined by solving the heat equation within the deposit as described in Sec. II D.

The latent heat  $H$  is 7.3 eV and  $J$  is taken from the measured deposition rates. Arc radius is assumed to be constant at 4 mm based on the measured deposit sizes and observations of craters on different sized anodes. With a total current of 65 A, this gives  $j_i = 1.2 \times 10^5 \text{ A/m}^2$  and  $j_{ee} = 1.2 \times 10^6 \text{ A/m}^2$ . Heat conduction is taken from the calculations in Sec. II D. The thermal conductivity of the helium-carbon plasma is taken from Ref. 29. The emissivity of graphite is taken to be 0.8.<sup>22</sup> The potential drop at the cathode sheath is taken as 3 V for the 6 mm anode<sup>21</sup> and 13 V for the 12 mm anode.<sup>13</sup>

The small cathode voltage drop for the 6 mm anode is due to the additional heating from deposition, reducing the importance of ion acceleration in heating the cathode, whereas 13 V is a typical value for a standard carbon arc.<sup>13</sup> Additionally, Ref. 17 has inferred the presence of an anode sheath for small anodes in order to support the enhanced ablation.

The results of our calculations are shown in Tables I and II for the 12 and 6 mm anodes, respectively, where the rows of the tables correspond to the labeled terms in Eq. (2). In view of the approximate nature of our calculations, the results have been rounded to lower precision, but this does not affect the overall conclusions. In both cases, energy balance is obtained to within the uncertainties of our calculations. For the 12 mm anode, cooling is dominated by electron emission and conduction through the deposit, while heating is dominated by conduction through the helium-carbon plasma. The important role of heat conduction from the plasma is similar to what has been observed in welding arcs.<sup>30</sup> Deposition plays a minor role. The radiation cooling for the arc with the 12 mm anode is smaller due to a smaller area on the cathode being at high temperatures based on Fig. 3.

With the 6 mm anode, deposition becomes a dominant term in the energy balance, while there is radiative cooling instead of heating due to the smaller anode surface. The calculated contribution due to deposition is likely an overestimate due to the presence of carbon complexes in the plasma, which has been inferred from the observation of their spectral lines in similar arcs.<sup>31</sup>

For the 12 mm anode, the main uncertainty is due to thermal conduction from the plasma. This is caused by the variable thermal conductivity of the carbon-helium plasma and the length scale over which the temperature falls. Our calculation assumes a drop from 7000 K to the cathode temperature over 1 mm, and estimates the heat flux by solving  $\nabla(\kappa\nabla T) = 0$  in one dimension, using the thermal conductivities tabulated in Ref. 29. With the 6 mm anode, the properties of the deposit become an additional complication as they affect the conduction losses through the cathode, as shown in Sec. II. Finally, this calculation does not include radiation from the plasma.

Even with the uncertainties, we are still able to account for the energy balance at the cathode to within 25% of the arc power in the two different regimes, as the additional

TABLE I. Energy balance using a 12 mm diameter anode. The uncertainty in conduction is found by varying deposit emissivity from 0 to 0.8 as shown in Sec. IID, while the uncertainty in plasma conduction is due to different plasma compositions used in the conductivity calculations. The numbers (1) to (7) correspond to the labeled terms in Eq. (2).

Energy source	Power (W)
(1) Ions	120
(2) Plasma conduction	$310 \pm 80$
(3) + (7) Net radiation	110
(4) Deposition	10
(5) Deposit conduction	$-(280 \pm 20)$
(6) Electrons	-290
Total	$-20 \pm 100$

TABLE II. Energy balance using a 6 mm diameter anode. The uncertainty in deposit conduction is due to the material properties of the deposit as discussed earlier. The range is determined by a parameter scan in  $\kappa$  and  $\epsilon$  which causes the calculated and observed surface temperatures to match.

Energy source	Power (W)
(1) Ions	60
(2) Plasma conduction	$310 \pm 80$
(3) + (7) Net radiation	-100
(4) Deposition	350
(5) Deposit conduction	$-(460 \pm 180)$
(6) Electrons	-290
Total	$-130 \pm 260$

heating due to deposition is balanced by changes in thermal conduction through the deposit and radiative losses.

Our results show that the anodic carbon arc can operate in two different ablation-deposition regimes based on the anode ablation and its contribution to the energy balance of the arc. The transition between the two regimes is likely due to the size of the plasma as compared to the anode diameter.<sup>17</sup> While the energy balance at the cathode in the arc with the 12 mm diameter anode may be similar to the that of the typical cathodic arc due to the low ablation, the situation when there is enhanced ablation is quite different.

Due to heating from deposition (i.e., latent heat), the role of ion heating at the cathode is not as important and does not require as large a voltage drop. This result appears to be consistent with the hypothesis of a positive anode sheath for small anodes.<sup>17</sup> For small anodes, the cathode voltage drop can be smaller while maintaining thermionic emission, while the remaining portion of the applied voltage can drop in the short plasma column and anode sheath. Here, it is assumed that the anode sheath attracts electrons rather than repelling them as could be in the case of the large anode.

#### IV. SUMMARY

Anodic carbon arc experiments were conducted between graphite anodes of various diameters and copper cathodes. The ablation rate decreased with increasing anode diameter before becoming small and approximately constant,<sup>17</sup> while the formation of the cathode deposit was found to be crucial in the operation of the arc.<sup>15</sup> The evaporation of the graphite anode and formation of the carbon deposit on the cathode are self-organized to maintain the current conduction in the arc.

We show that for smaller anodes, the contribution of the deposition to energy balance must be included when modelling the arc-cathode interaction due to the large ablation and deposition rates. The differences in the ablation rate when increasing the diameter suggest that the arc can operate in two different ablation-deposition regimes, which cannot be captured by current models because of the contribution of latent heat. As the yield of nanomaterials is determined by ablation rate, the inclusion of energy balance is relevant to nanosynthesis. This may be also applicable to other anodic arcs with a solid deposit and should be a subject for further experimental and simulation work.

## ACKNOWLEDGMENTS

We would like to thank Mr. Alex Merzhevskiy, Mr. Enrique Merino for technical support, Dr. Travis Gray for assisting with infrared measurements, Dr. Andrei Khodak, Dr. Michael Keidar, Dr. Igor Kaganovich, Mr. Emre Türkoz and Mr. Yao-Wen Yeh for fruitful discussions. This work was supported by U.S. Department of Energy, Office of Science, Basic Energy Sciences, Materials Sciences and Engineering Division.

- <sup>1</sup>Y. Raizer, *Gas Discharge Physics* (Springer-Verlag, 1991).
- <sup>2</sup>M. R. Null and W. W. Lozier, *J. Opt. Soc. Am.* **52**, 1156 (1962).
- <sup>3</sup>M. R. Null and W. W. Lozier, *Rev. Sci. Instrum.* **29**, 163 (1958).
- <sup>4</sup>S. Iijima *et al.*, *Nature* **354**, 56 (1991).
- <sup>5</sup>C. Journet, W. Maser, P. Bernier, A. Loiseau, M. L. De La Chapelle, d. l. S. Lefrant, P. Deniard, R. Lee, and J. Fischer, *Nature* **388**, 756 (1997).
- <sup>6</sup>A. Mansour, M. Razafinimanana, M. Monthoux, M. Pacheco, and A. Gleizes, *Carbon* **45**, 1651 (2007).
- <sup>7</sup>D. T. Colbert, J. Zhang, S. M. McClure, P. Nikolaev, Z. Chen, J. H. Hafner, D. W. Owens, P. G. Kotula, C. B. Carter, J. H. Weaver, A. G. Rinzler, and R. E. Smalley, *Science* **266**, 1218 (1994).
- <sup>8</sup>M. Keidar, A. Shashurin, J. Li, O. Volotskova, M. Kundrapu, and T. S. Zhuang, *J. Phys. D: Appl. Phys.* **44**, 174006 (2011).
- <sup>9</sup>R. H. Baughman, A. A. Zakhidov, and W. A. de Heer, *Science* **297**, 787 (2002).
- <sup>10</sup>E. T. Thostenson, Z. Ren, and T.-W. Chou, *Compos. Sci. Technol.* **61**, 1899 (2001).
- <sup>11</sup>M. Meyyappan, *Carbon Nanotubes: Science and Applications* (CRC press, 2004).
- <sup>12</sup>D. Tang, L. Sun, J. Zhou, W. Zhou, and S. Xie, *Carbon* **43**, 2812 (2005).
- <sup>13</sup>M. Keidar and I. I. Beilis, *J. Appl. Phys.* **106**, 103304 (2009).
- <sup>14</sup>W. L. Upson, *Proc. Phys. Soc. London* **21**, 1 (1907).
- <sup>15</sup>J. Ng and Y. Raitses, *Carbon* **77**, 80 (2014).
- <sup>16</sup>Z. Weng-Sieh, K. Cherrey, N. G. Chopra, X. Blase, Y. Miyamoto, A. Rubio, M. L. Cohen, S. G. Louie, A. Zettl, and R. Gronsky, *Phys. Rev. B* **51**, 11229 (1995).
- <sup>17</sup>A. J. Fetterman, Y. Raitses, and M. Keidar, *Carbon* **46**, 1322 (2008).
- <sup>18</sup>A. Shashurin and M. Keidar, *Carbon* **46**, 1826 (2008).
- <sup>19</sup>P. M. Ajayan, P. Redlich, and M. Rhle, *J. Mater. Res.* **12**, 244 (1997).
- <sup>20</sup>Y. Saito, T. Yoshikawa, S. Bandow, M. Tomita, and T. Hayashi, *Phys. Rev. B* **48**, 1907 (1993).
- <sup>21</sup>N. Alekseyev and G. Dyuzhev, *Tech. Phys.* **46**, 1247 (2001).
- <sup>22</sup>A. Ostrogorsky and C. Marin, *Heat Mass Transfer* **42**, 470 (2006).
- <sup>23</sup>R. W. Powell and F. H. Schofield, *Proc. Phys. Soc.* **51**, 153 (1939).
- <sup>24</sup>Y. Raitses, C. Skinner, F. Jiang, and T. Duffy, *J. Nucl. Mater.* **375**, 365 (2008).
- <sup>25</sup>A. Drenik, A. Vesel, and M. Mozetič, *J. Nucl. Mater.* **386–388**, 893 (2009).
- <sup>26</sup>W. Hurler, M. Pietralla, and A. Hammerschmidt, *Diamond Relat. Mater.* **4**, 954 (1995).
- <sup>27</sup>M. S. Benilov and A. Marotta, *J. Phys. D: Appl. Phys.* **28**, 1869 (1995).
- <sup>28</sup>A. Anders, *Cathodic Arcs: From Fractal Spots to Energetic Condensation* (Springer, 2008).
- <sup>29</sup>W. Wang, M. Rong, A. B. Murphy, Y. Wu, J. W. Spencer, J. D. Yan, and M. T. C. Fang, *J. Phys. D: Appl. Phys.* **44**, 355207 (2011).
- <sup>30</sup>P. Zhu, J. J. Lowke, and R. Morrow, *J. Phys. D: Appl. Phys.* **25**, 1221 (1992).
- <sup>31</sup>H. Lange, K. Saidane, M. Razafinimanana, and A. Gleizes, *J. Phys. D: Appl. Phys.* **32**, 1024 (1999).